Late Variscan metamorphic and magmatic evolution in the eastern Pyrenees revealed by U–Pb age zircon dating

CARMEN AGUILAR[1*], MONTSERRAT LIESA[1], PEDRO CASTIÑEIRAS[2] & MARINA NAVIDAD[2]

[1]*Departament de Geoquímica, Petrologia i Prospecció Geològica, Facultat de Geologia, Universitat de Barcelona (UB), Zona Universitària de Pedralbes, Martí i Franquès s/n, 08028 Barcelona, Spain*

[2]*Departamento de Petrología y Geoquímica, Facultad de Ciencias Geológicas, Universidad Complutense de Madrid, José Antonio Novais 12, 28040 Madrid, Spain*

**Corresponding author (e-mail: carmenmaguilar@ub.edu)*

Abstract: Variscan migmatites cropping out in the eastern Pyrenees were dated together with Late Variscan plutonic rocks. Upper Proterozoic–Lower Cambrian series were migmatized during a thermal episode that occurred in the interval 320–315 Ma coeval with the main Variscan deformation event (D_1). The calc-alkaline Sant Llorenç–La Jonquera pluton and the gabbro–diorite Ceret stock were emplaced during a later thermal episode synchronous with the D_2 deformation event. A tonalite located at the base of La Jonquera suite intruded into the upper crustal levels between 314 and 311 Ma. The gabbro–diorite stock was emplaced in the middle levels of the series in two magmatic pulses at 312 and 307 Ma. The thermal evolution recorded in the eastern Pyrenees can be correlated with that of neighbouring areas of NE Iberia (Pyrenees–Catalan Coastal Ranges) and SE France (Montagne Noire). The correlation suggests a NW–SE-trending zonation where the northeasternmost areas (Montagne Noire and eastern Pyrenees) would occupy relatively more internal zones of the orogen than the southwesternmost ones.

The eastern Pyrenees (Fig. 1a) are a typical example of Variscan metamorphic basement in southwestern Europe (Fig. 1b), where the pre-Variscan series was deformed by polyphase deformation and metamorphosed under low-pressure–high-temperature conditions during the Late Mississippian to Pennsylvanian (e.g. Zwart 1962; Guitard *et al.* 1995). Crustal melting took place in the middle and lower crust and was synchronous with the intrusion of late Variscan granitoids into upper crustal levels (e.g. Debon *et al.* 1995; Roberts *et al.* 2000; Vilà *et al.* 2005). Since the pioneering work of Zwart and Guitard the timing and the geodynamic context of this thermal evolution has still not been resolved.

The aim of this paper is to constrain the timing of the Variscan thermal evolution in the Roc de Frausa Massif (Fig. 1c) between the formation of the early regional orogenic migmatites and the emplacement of the upper and middle crustal intrusive rocks. Few geochronological data on migmatites are available in the Pyrenees at present. In addition, ages from the intrusive rocks need to be revised as earlier attempts using the Rb–Sr method have yielded younger emplacement ages of 282 ± 5 Ma (Cocherie 1984) and more recent U–Pb zircon data have given 295 ± 7 Ma (Maurel 2003). However, the U–Pb method has yielded intrusion ages between 314 and 301 Ma in other adjacent plutons of the Pyrenees.

New U–Pb dating of zircon using sensitive high-resolution ion microprobe-reverse geometry (SHRIMP-RG) was carried out on Variscan migmatites together with dating of Late Variscan plutonic rocks emplaced at different crustal levels. These data are combined with trace element chemistry on zircon and textures revealed by cathodoluminescence (CL). The resulting age data and the relative ages of the tectonic–metamorphic and magmatic processes allow us to make a better interpretation of the late Variscan thermal evolution and to attempt a first correlation with the neighbouring areas.

Geological setting

The approximately east–west-trending antiformal dome-shaped (Fig. 1c) Roc de Frausa Massif forms a distinctive geological assemblage separated from neighbouring areas (e.g. Albera, Aspres and Canigó massifs) by Alpine faults. Its pre-Variscan metasedimentary and metaigneous rocks (see details and age data given by Autran & Guitard 1969; Castiñerias *et al.* 2008) are embedded in the Variscan Sant Llorenç–La Jonquera plutonic complex. This coherent block was uplifted in response to Palaeogene compression and subsequent Neogene extensional tectonics, favouring the outcropping of the lowermost materials (Cirés *et al.* 1994).

The pre-Variscan gneisses and metasediments were affected by a third phase of deformation events (Liesa & Carreras 1989). The main deformation event (D_1) is characterized by the development of a pervasive foliation (S_1), representing the axial plane of a tightly folded foliation (S_0). Two later deformational events (D_2 and D_3) produced a fold interference pattern that resulted in the present structure of the massif (Fig. 1c). D_2 is characterized by NE–SW-trending tight folds that, in high-strain domains, transpose S_1 foliation. D_3 is recognized by NW–SE-trending open folds and by shear zones related to it. A pervasive retrograde foliation developed in these shear zones transposed older ones. D_1 and D_2 are attributed to the Variscan orogeny and are correlated with prograde metamorphism, whereas D_3 was produced in greenschist conditions and can be related either to the late Variscan or to the Alpine cycle.

The intensity of metamorphic overprint increased from amphibolite-facies (andalusite micaschists in the higher levels to sillimanite micaschists in the medium levels) to lower granulite-facies conditions towards the deeper structural levels (Liesa & Carreras

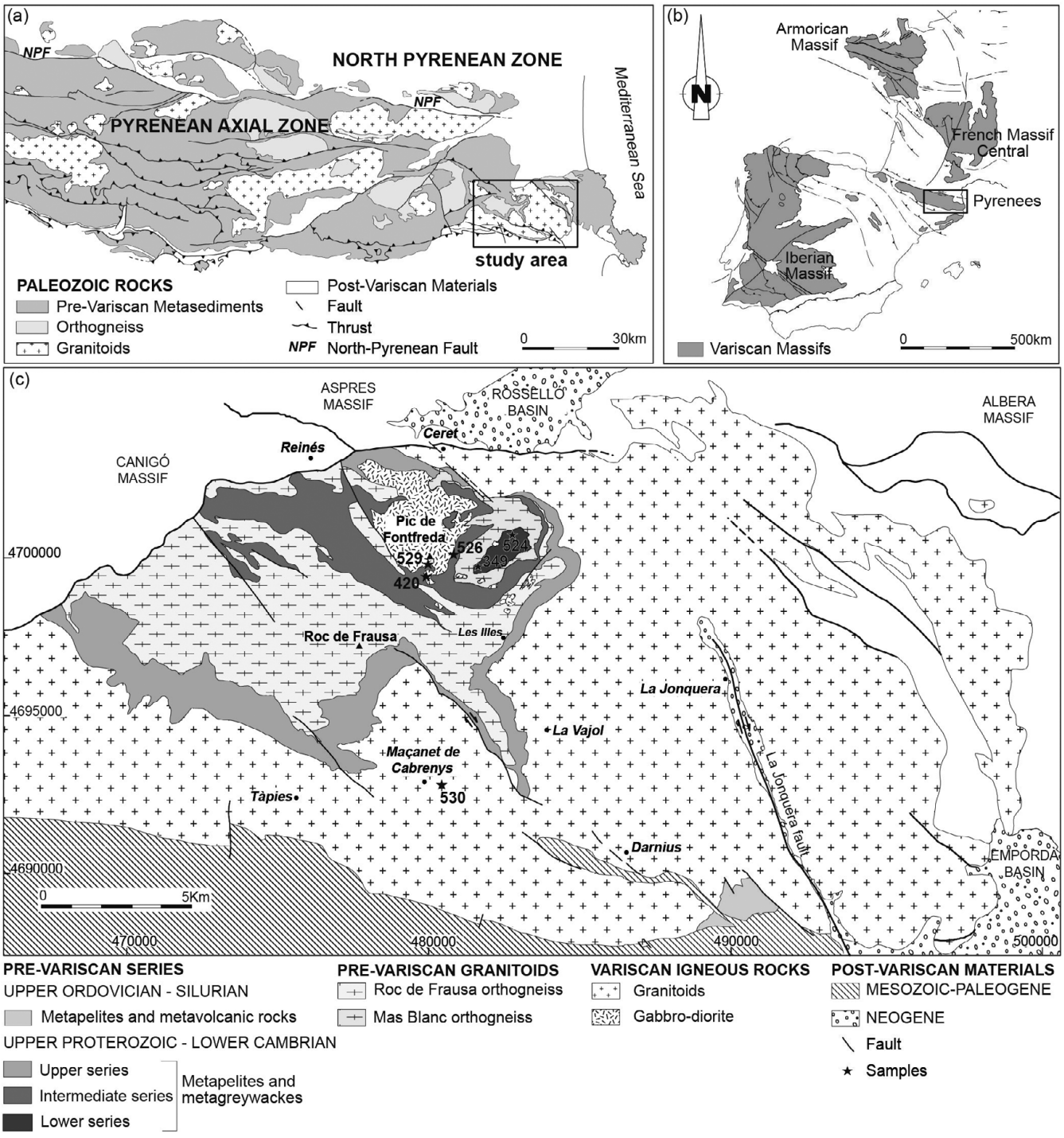

Fig. 1. Geological sketch maps of the Variscan basement in (**a**) the central and eastern Pyrenees and (**b**) central and southwestern Europe. (**c**) Geological sketch map of the Roc de Frausa Massif and Sant Llorenç–La Jonquera plutonic complex with the location of the samples collected.

1989), where widespread migmatization took place. The lowermost migmatites reached temperature peak conditions during the main deformational event (D_1).

The late Variscan magmatic bodies were emplaced in different levels of the pre-Variscan rock series (Liesa & Carreras 1989). The Sant Llorenç–La Jonquera batholith is a sheet-like intrusion, varying in composition from tonalite to granite. Although the base of the batholith was emplaced roughly parallel to lithological boundaries and S_1 foliation between the Upper Proterozoic–Lower Cambrian series and the Upper Ordovician–Silurian rocks (Fig. 1c), it displays a cross-cutting relationship with the country-rock at its eastern end and at the roof (Fig. 1c).

The Ceret stock is the most prominent of a series of smaller (10 km^2) gabbro–diorite bodies including ultramafic cumulates intruded into the intermediate series. Both the Sant Llorenç–La Jonquera batholith and the Ceret stock are synkinematic with the D_2 deformation event, as indicated by the preferred orientation of the magmatic fabric. They have different geochemical characteristics

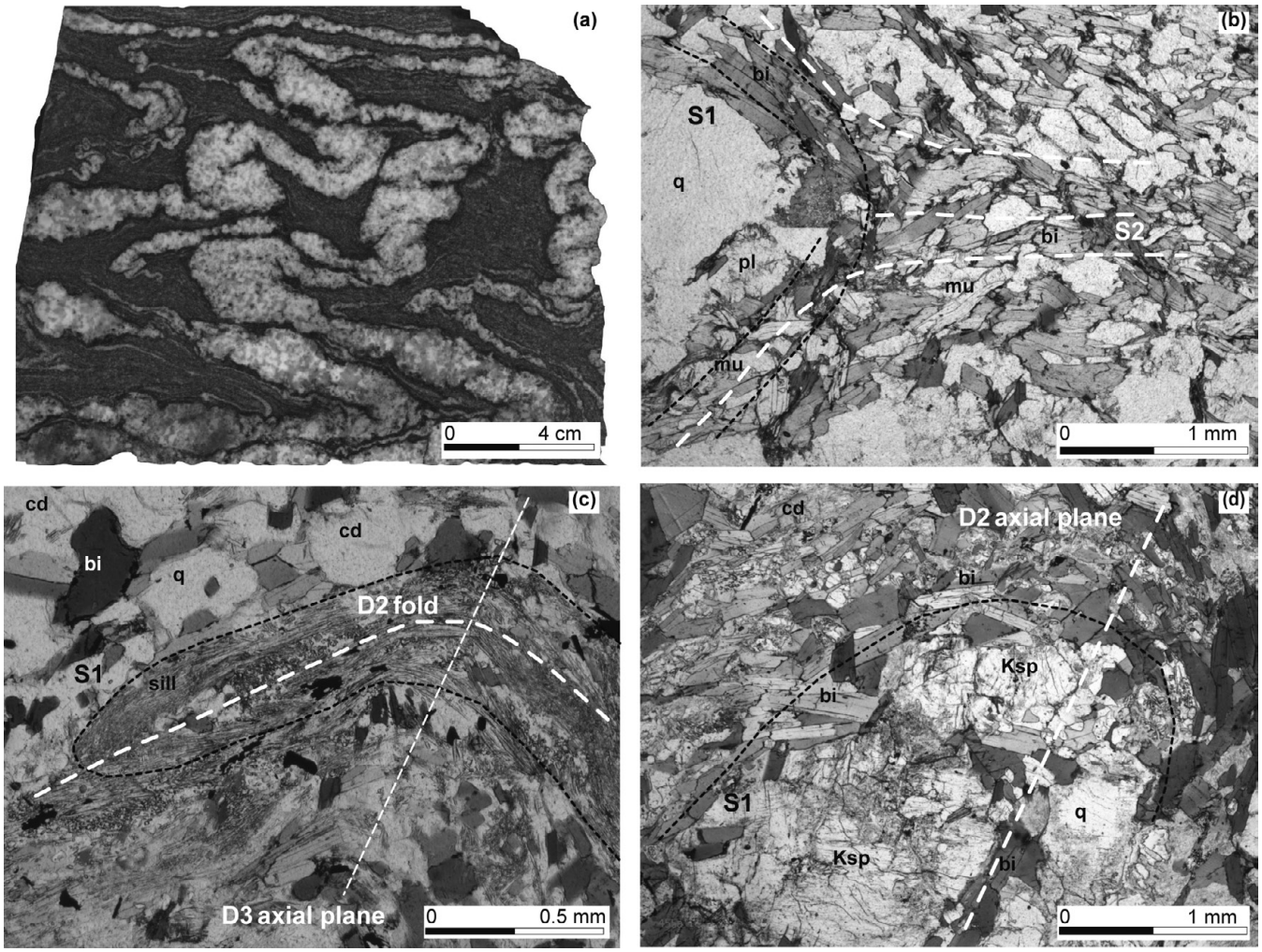

Fig. 2. Microscopic aspect of the migmatites. Sample 349 (lowermost migmatites): (**a**) tightly folded lithological banding; (**b**) muscovite and biotite define the S_1 foliation and crystallize parallel to the axial planes of tight D_2 folds. Sample 526 (migmatites from the Ceret stock contact aureole): (**c**) fibrolite defines S_1 folded by subsequent D_2 deformation event that developed tight folds, which are also folded by the last deformation event (D_3); (**d**) S_2 is defined by the crystallization of the neosome parallel to the axial plane of the folds. Mineral abbreviations after Holland & Powell (1998).

and belong to two genetically distinct igneous suites produced in different levels of the lithosphere (Vilà *et al.* 2005). Cordierite–andalusite hornfelses formed around the Sant Llorenç–La Jonquera intrusion, whereas widespread migmatization in the granulite facies developed in the contact metamorphic aureole around the Ceret stock, including a mineral association of garnet, cordierite, biotite, sillimanite, K-feldspar, plagioclase and quartz roughly aligned parallel to the axial planes of D_2 folds (Fig. 2c and d).

Sample description

To determine the time evolution from early migmatization to the emplacement of the magmatic bodies and the formation of migmatites around the gabbro–diorite Ceret stock (Fig. 1c), we selected (1) two migmatites from the lower series, (2) two late Variscan igneous rocks, and (3) two migmatites from the contact aureole.

The two migmatites from the lower series (samples 349 and 524) show a tightly folded lithological banding (Fig. 2a) with a coarse-grained (>1 mm) leucosome and a fine-grained (<1 mm) palaeosome. The latter displays a granolepidoblastic texture and preserves S_1 foliation. The mineral association in sample 349 consists of quartz, plagioclase, muscovite and biotite, and the accessories, zircon, monazite, tourmaline and opaque minerals. Muscovite and biotite are subhedral and define S_1 foliation. Locally, biotite and muscovite crystallize parallel to the axial planes of tight D_2 folds (Fig. 2b). Retrograde chlorite, epidote and sericite are related to D_3 structures. In sample 524, the characteristic mineral association contains quartz, plagioclase and biotite. Ilmenite, magnetite, zircon, monazite, apatite and tourmaline are found as accessory minerals. Isolated grains of garnet are included in plagioclase. Most of the subidioblastic biotite crystals are located in the palaeosome and define a preferred orientation parallel to S_1. This foliation developed open folds during a D_3 deformation. Occasionally, kink bands are formed in biotite and their axial planes are also related to the D_3 deformation event.

Sample 530 is a holocrystalline, granular tonalite from the Sant Llorenç–La Jonquera batholith with the major constituents quartz, K-feldspar, plagioclase, biotite and hornblende and with variable grain size. Plagioclase forms idiomorphic phenocrysts and displays oscillatory zoning as well as Carlsbad and polysynthetic twinning. Biotite and hornblende are subhedral and show a strong pleochroism from brown to reddish brown and green to light brown, respectively. Biotite crystals contain a large number of inclusions of zircon and apatite. Opaque ore and allanite are also present. Sample 420, represents a medium- to coarse-grained gabbro from the Ceret

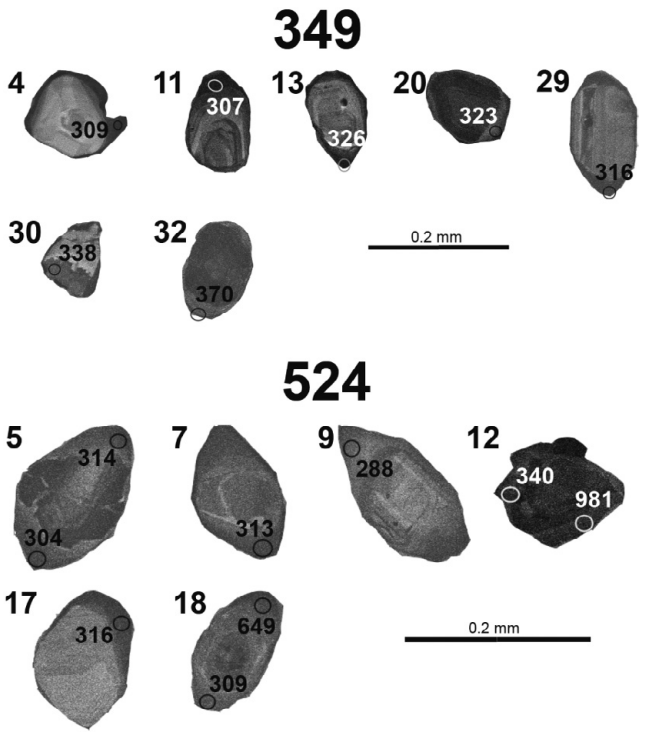

Fig. 3. CL images of the analysed zircon rims from the lowermost migmatites (samples 349 and 524) with the location of the SHRIMP spots.

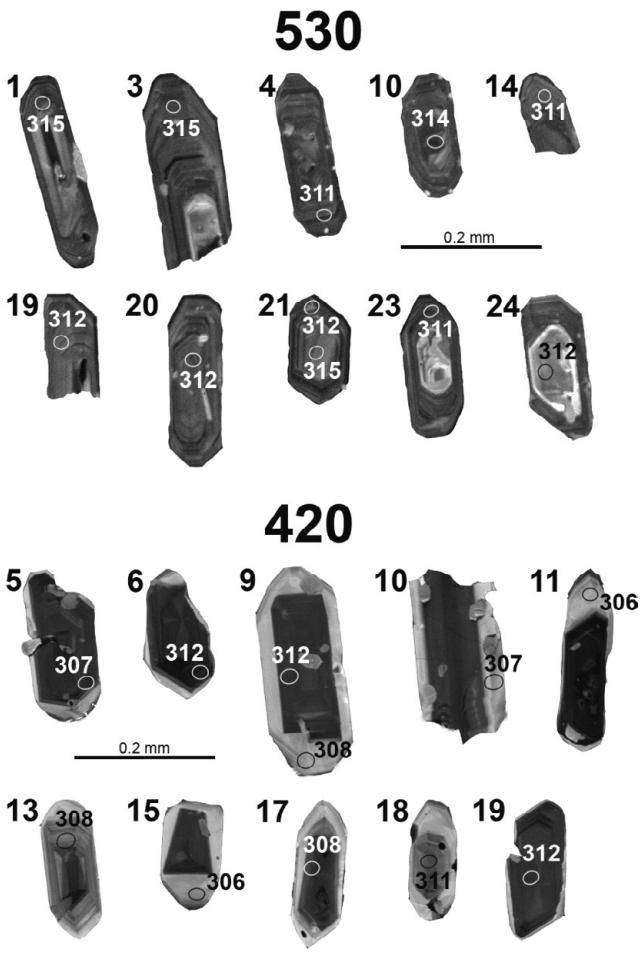

Fig. 4. CL images of the analysed zircons from the Sant Llorenç–La Jonquera tonalite (samples 530) and the Ceret stock gabbro (sample 420) with the location of the SHRIMP spots.

stock with variable grain size. It has a granular to ophitic texture and it is composed of clinopyroxene, amphibole, plagioclase, biotite and the accessories zircon, apatite and opaque ore. Quartz is scarce and has an interstitial texture. Plagioclase is idiomorphic with Carlsbad and polysynthetic twinning and is surrounded by clinopyroxene, amphibole and anhedral biotite. Altered olivine is locally included in clinopyroxene. Amphibole and biotite occasionally display a coronitic texture around clinopyroxene. Secondary minerals are iddingsite, white mica and uralite.

Samples 526 and 529 represent migmatites from the Ceret stock contact aureole corresponding to metapelitic rocks from the intermediate series located near the Pic de Fontfreda. Both samples consist of a coarse-grained leucosome and a fine-grained palaeosome. In sample 526, the leucosome has a granular texture composed of quartz, K-feldspar, biotite and idiomorphic to subidiomorphic porphyroblasts of plagioclase, garnet and cordierite. The palaeosome shows a grano-lepidoblastic banded texture with xenoblastic quartz and plagioclase layers alternating with fibrolite and biotite layers. Sillimanite is either fibrolitic or prismatic and is included in garnet and cordierite porphyroblasts together with biotite and ilmenite. Sillimanite is found in three textural situations, thus allowing us to establish the blastesis–deformation relationships: type I appears as fibrolite in the fold flanks of the first schistosity (S_0); type II is also fibrolitic and defines S_1 (Fig. 2c); type III is coarse prismatic sillimanite parallel to the S_2 foliation. Cordierite porphyroblasts display simple twinning. Accessory minerals are ilmenite, pyrite, apatite, zircon and monazite. In sample 529, the leucosome is also composed of quartz, antiperthitic plagioclase, biotite, garnet, cordierite and the accessories spinel (included in cordierite), ilmenite, pyrite, apatite, zircon and monazite. The palaeosome is formed of alternating xenoblastic quartzofeldspathic and biotite layers. Cordierite is also found as porphyroblasts. Quartz, plagioclase and biotite from the palaeosome crystallize parallel to the S_1 foliation. A second foliation (S_2) is defined by the crystallization of the leucosome parallel to the axial plane of the folds and associated with the D_2 deformation event (Fig. 2d). Cordierite porphyroblasts include biotite oriented by S_1 and S_2, which is interpreted as late to post-D_2 deformation. Sericite, pinnite and muscovite are retrograde minerals.

Zircon morphology

Migmatites from the lower series

Zircons obtained from the lowermost migmatites (samples 349 and 524) are small and scarce. In fact, fewer than a hundred grains were extracted from *c.* 12 kg of each sample. Zircon grains can be colourless or various shades of brown and purple, and are practically free of visible inclusions. Two groups of zircon can be distinguished: (1) subrounded stubby grains with pitted and dull surfaces owing to sedimentary abrasion that are interpreted as detrital zircon; (2) idiomorphic grains with highly variable habits and secondary and shiny faces that are interpreted as metamorphic zircon. No evidence was found of chemically corroded grains without further overgrowths. CL images of the latter reveal a varied population of cores with scarce irregular dark rims (Fig. 3). The cores have different textures, including oscillatory, sector and soccer-ball zoning, and contrasting luminescence responses, from low to high. These characteristics suggest that the

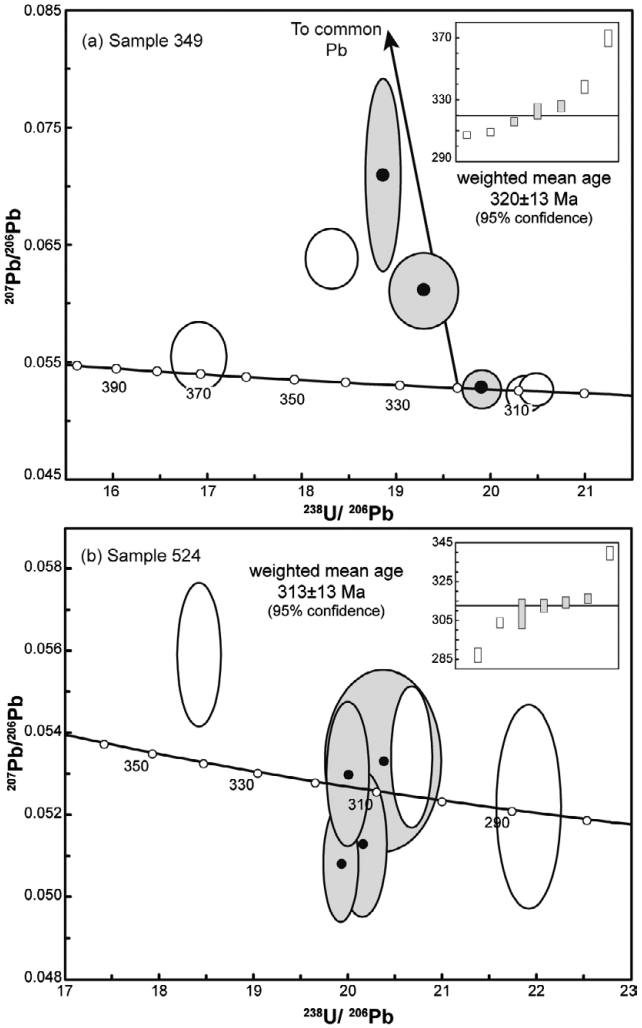

Fig. 5. Tera–Wasserburg diagrams of SHRIMP U–Pb zircon ages from the lowermost migmatites: (**a**) sample 349; (**b**) sample 524. The grey-shaded ellipses represent the data used to obtain the weighted mean age (inset), whereas the white ellipses were discarded. Inherited ages are not shown for clarity. Error ellipses are ±2σ.

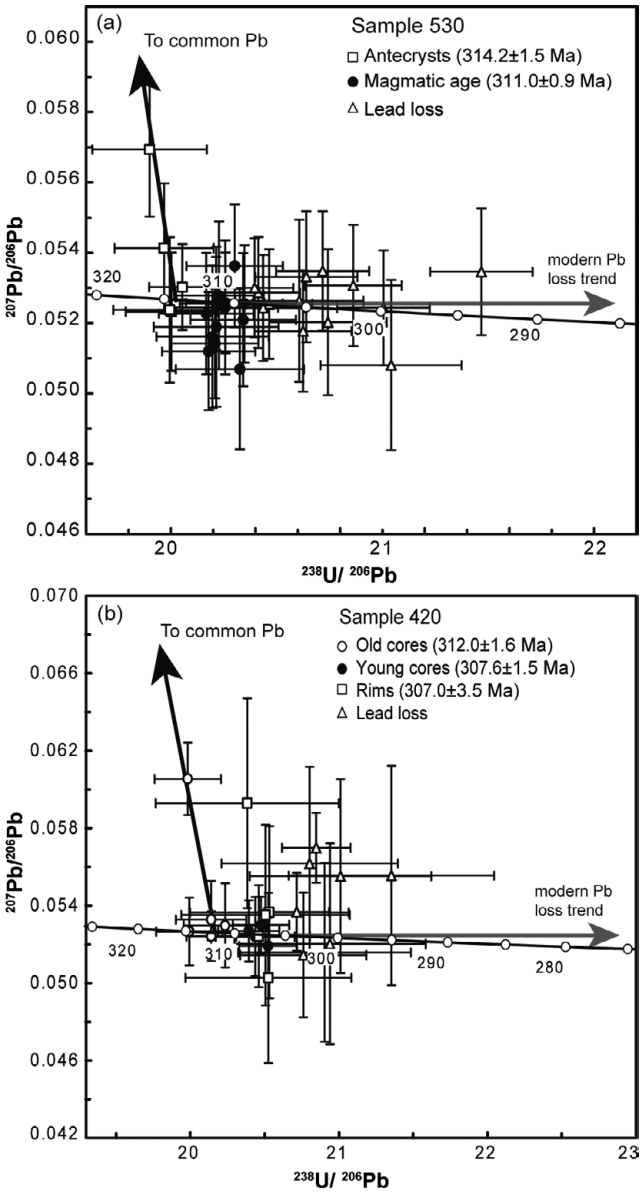

Fig. 6. Tera–Wasserburg diagrams of zircon U–Pb ages from Variscan igneous rocks: (**a**) the Sant Llorenç–La Jonquera tonalite (sample 530); (**b**) the Ceret stock gabbro (sample 420). Error crosses are ±2σ.

cores represent former detrital grains, magmatic in origin, which are overgrown during metamorphism.

Sant Llorenç–La Jonquera tonalite and Ceret stock gabbro

Zircon crystals from the tonalite of the Sant Llorenç–La Jonquera batholith (sample 530) are colourless, pale yellow or light purple and contain few visible inclusions. They form short prisms with differently shaped pyramid terminations and length-to-breadth ratios between 1:2 and 1:4. Under CL, zircons display broad moderately luminescent oscillatory zones typical of magmatic environments, and in a few grains less luminescent homogeneous cores can also be discerned (Fig. 4).

Zircons from the Ceret stock gabbro (sample 420) are moderately elongated prisms with rounded terminations, variable aspect ratios (1:1 to 1:3) and abundant inclusions. They are generally broken. CL images reveal definite core–rim structures that can be observed even under the transmitted light microscope. The cores exhibit a non-luminescent weakly oscillatory and sector zoning surrounded by variably thick rims (*c.* 25 μm thick) that are highly luminescent and display a subtle broad oscillatory zoning (Fig. 4).

Migmatites from the Ceret stock contact aureole

Only one of the migmatites from the Ceret stock contact aureole produced a zircon yield (sample 529), whereas sample 526 was devoid of this mineral. As in the lowermost migmatites, zircon grains are variably coloured and display two distinct morphologies: one corresponding to detrital zircon and the other to metamorphic zircon.

Results

Zircon U–Pb dating

Analytical results for zircon U–Pb dating are plotted in Figures 5 and 6. The uncertainties for the error ellipses and crosses are

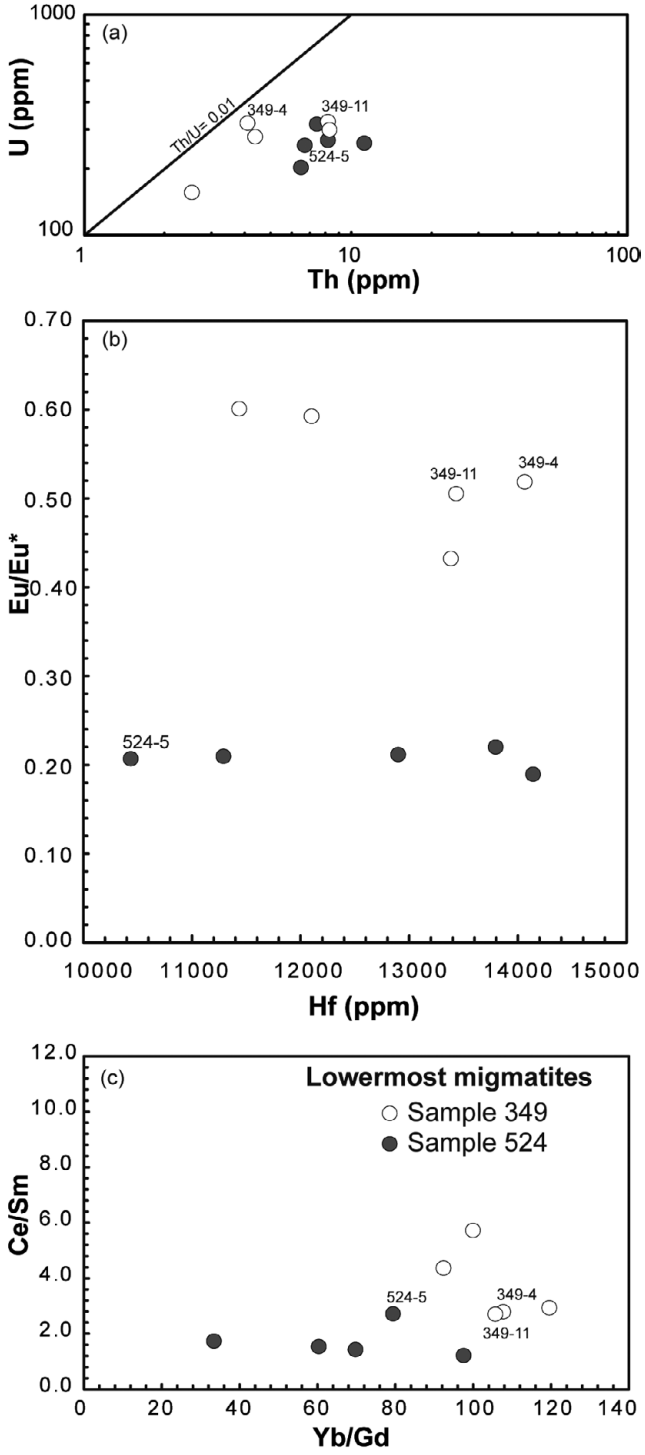

Fig. 7. Compositional diagrams for zircon from the lowermost migmatites (samples 349 and 524): (**a**) U v. Th; (**b**) Hf v. Eu/Eu*; (**c**) Yb/Gd v. Ce/Sm. The labelled analyses are those not used to obtain the mean age.

represented at the 2σ level. Depending on the amount of data, the mean square weighted deviation (MSWD) has to be lower than a theoretical value to confirm the statistical validity of the calculated age (Wendt & Carl 1991). Ages younger than 1000 Ma are reported using the 207-corrected $^{206}Pb/^{238}U$ ratio, whereas older ages are reported using the 204-corrected $^{207}Pb/^{206}Pb$ ratio.

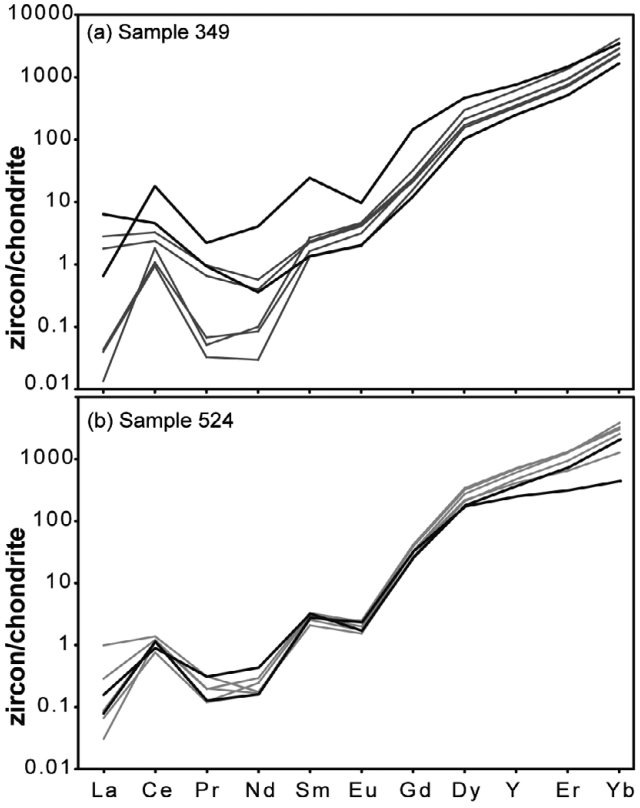

Fig. 8. Chondrite-normalized REE patterns for sample 349 (**a**) and sample 524 (**b**). Chondrite normalization according to Anders & Grevesse (1989), modified by Korotev (1996).

Migmatites from the lower series. In sample 349, a total of 37 analyses were performed on 36 zircon grains. Areas with clear magmatic textures were avoided, as they could represent inherited zones, so all the analyses were focused on rims or areas with homogeneous zoning that were presumably metamorphic. However, only seven analyses yielded ages younger than 400 Ma, whereas the remaining 30 spots yielded ages between 600 and 2740 Ma, which were interpreted as inheritance. Owing to the scatter in the young ages (Fig. 5a, inset), obtaining a valid age from these seven analyses is difficult. We can consider the two oldest analyses in this group as outliers, and calculate the weighted average with the remaining five analyses. However, the high MSWD obtained in this calculation (26) indicates that these data do not represent a consistent population. The best statistical estimate is obtained anchoring only three data to a common Pb composition of 0.857, giving a younger intercept age of 320 ± 13 Ma (Fig. 5a). Once again, the high MSWD value (9.9) indicates that the considered analyses do not constitute a consistent population, so this number must be regarded only as the upper limit for the age of metamorphism.

In sample 524, a total of 22 spot analyses also located at the rims were carried out on 20 zircon grains. Only seven analyses yielded Variscan ages, *sensu lato* (i.e. less than 340 Ma). In this case, the two extreme values can be regarded as clear outliers (Fig. 5b, inset), and we calculate the weighted average using the rest of the analyses. Once more, the result produces a high MSWD (13) that can be considerably lowered if we consider only four spots to calculate the weighted mean, resulting in an age of 315 ± 4 Ma, with an acceptable MSWD value (2.0; Fig. 5b). The rest of the analyses yielded inherited ages between 650 and 2660 Ma.

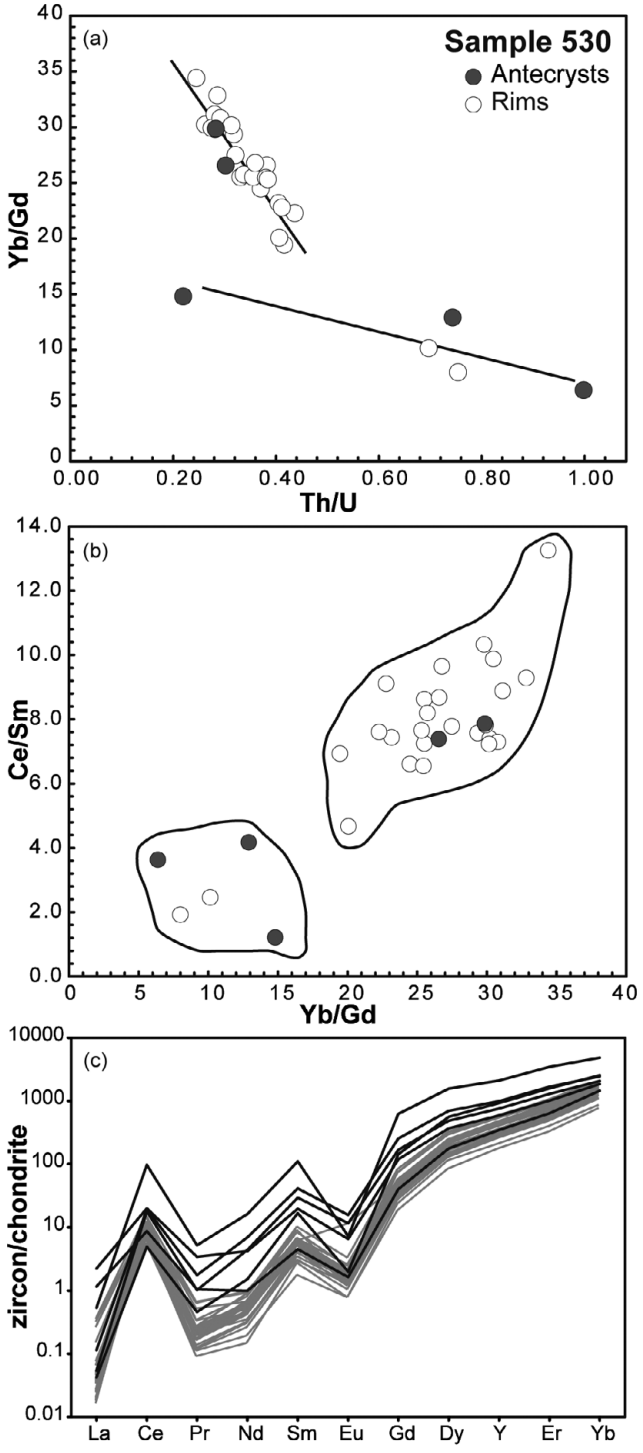

Fig. 9. Compositional diagrams for zircon from the Sant Llorenç–La Jonquera tonalite (sample 530): (**a**) Th/U v. Yb/Gd plot; (**b**) Yb/Gd v. Ce/Sm plot; (**c**) chondrite-normalized REE patterns. Chondrite normalization as in Figure 8.

Sant Llorenç–La Jonquera tonalite and Ceret stock gabbro. In sample 530 (a tonalite from the Sant Llorenç–La Jonquera batholith), 31 spot analyses were performed on 30 zircon grains. Single results range between 315 and 293 Ma. Taking into account the CL texture of the zircon grains, most of the cores yielded the oldest ages, whereas data from the rims were usually younger. The best estimate for the age of the cores was obtained from five analyses (Fig. 6a) yielding a mean age of 314.2 ± 1.5 Ma, with an MSWD of 0.11. Two of these analyses had moderate common Pb contents and were connected with the concordant analyses by means of a line anchored to a common Pb composition of 0.857. As regards the rims, a reliable estimation for their age was obtained from 13 analyses, yielding a mean age of 311.0 ± 0.9 Ma with an MSWD of 0.38. The remaining 13 analyses represented ages younger than 308 Ma and were probably attributed to variable radiogenic Pb loss as they were obtained from both cores and rims. The difference in age between cores and rims suggests that the former might represent antecrysts (Charlier *et al.* 2005); that is, crystals formed slightly earlier on the crystallization path.

In sample 420 (a gabbro from the Ceret stock), 24 spots were analysed on 19 zircons with clear core–rim structures. The data were evenly distributed between 315 and 294 Ma (Fig. 6b), with the cores usually older than the rims. The weighted mean obtained from the 12 core analyses (*c*. 309 Ma) had a high MSWD, suggesting that the data contained more than one age population. In a further appraisal, we used the Sambridge & Compston (1994) approach to extract these age populations, considering the core analyses that were unaffected by Pb loss. By doing so, two age groups were established, namely an older one of 312.0 ± 1.6 Ma (MSWD = 0.15 for four analyses) and a younger one of 307.6 ± 1.5 Ma (MSWD = 0.24 for five analyses). As regards the rim analyses, the six younger values were clearly affected by Pb loss (Fig. 6b). However, the best estimate for their ages was obtained from four other analyses, yielding a mean age of 307.0 ± 3.5 Ma with an MSWD of 0.10.

Migmatites from the Ceret stock contact aureole. In sample 529, a total of 17 spot analyses were carried out in the same number of zircon grains, focusing on the rims or areas with zoning that could be attributed to metamorphic zircon. The ages vary between 570 and 2700 Ma and were interpreted as inheritance.

Zircon U, Th, Hf and REE composition

U, Th, Hf and trace element composition of zircon was used to gain insight into their petrogenesis and the analytical results are plotted in Figures 7–10. The interpretation of the results presented here will be discussed in the next section.

Migmatites from the lower series. Uranium concentrations in both migmatites (samples 349 and 524) are similar and range from 250 to 1100 ppm (Fig. 7a). Thorium contents range between 2.5 and 8 ppm in sample 349, whereas sample 524 has slightly higher values. In Figure 7a, both samples define a compact cluster around the 0.01 Th/U ratio and the concentration of hafnium (Fig. 7b) in both migmatites is comparable. By contrast, the Eu/Eu* anomaly is lower in sample 524 than in sample 349. Yb/Gd values (Fig. 7c) range between 35 and 120, with the lowest values corresponding to sample 524. The difference in the Ce/Sm ratio in both samples is small, with sample 349 having slightly higher values. In the REE chondrite-normalized diagram (Fig. 8a and b), the patterns defined by the migmatite samples are typical of high-grade and magmatic zircon, with a progressive fractionation from the heavy to the light REE and two prominent anomalies in cerium (positive) and europium (negative).

Sant Llorenç–La Jonquera tonalite and Ceret stock gabbro. In sample 530, the compositional difference between antecryst and rim analyses, including those affected by Pb loss, is discernible in only some elements and elemental ratios. In Figure 9a, analyses define

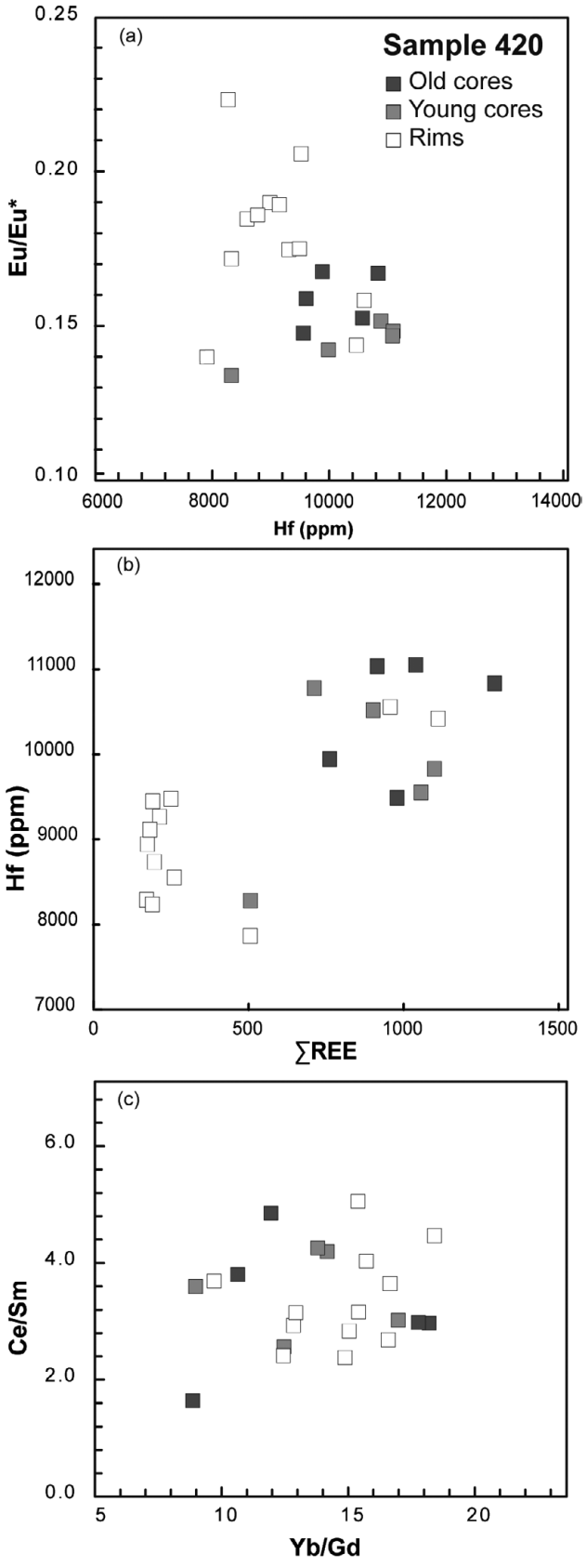

Fig. 10. Compositional diagrams for zircon from the Ceret stock gabbro (sample 420): (**a**) Hf v. Eu/Eu* plot; (**b**) ∑REE v. Hf plot; (**c**) Yb/Gd v. Ce/Sm plot.

two distinct trends; three out of five antecryst and two rim analyses have a gentle negative slope, whereas the rest of the analyses define a steeper negative slope. In Figure 9b, there is a positive correlation between the two ratios. The analyses cluster in two groups: one of the groups with three antecryst and two rim analyses at the low Yb/Gd–Ce/Sm end, and the other group with the remaining analyses at the high Yb/Gd–Ce/Sm end. In a chondrite-normalized plot (Fig. 9c), the rims (grey lines) show relatively homogeneous patterns, whereas core analyses (black lines) have heterogeneous patterns with variable Eu and Ce anomalies.

In sample 420, the compositional differences between the cores and the rims are more pronounced. In Figure 10a, the data define a negative correlation, with cores having a higher Hf content and lower values for the Eu anomaly than rims. In Figure 10b, the correlation of the data is positive, with the rims depleted in REE and Hf with respect to the cores. Furthermore, there is also a slight difference between the old and the young cores. By contrast, other compositional ratios such as the Ce/Sm and Yb/Gd ratios do not show marked variations. This is evident in Figure 10c, where the core and rim patterns are identical and the only difference is the lower content in REE of the rims with respect to the cores.

Summary and discussion

Timing of the Variscan thermal evolution in the eastern Pyrenees

Summarizing the results obtained, a late Variscan thermal evolution is recorded in the eastern Pyrenees involving two distinct processes, an early migmatization and a late intrusion of igneous rocks.

The earliest migmatization was coeval with the main deformation (D_1). It is recorded in the deepest levels of the Upper Proterozoic to Lower Cambrian series of the Roc de Frausa Massif. The Variscan partial melting history of the migmatites is poorly constrained by zircon geochronology as zircon recrystallization is generally limited to thin discontinuous rims. Nevertheless, the onset of crustal melting can be estimated to have occurred between 320 ± 13 and 315 ± 4 Ma (Serpukhovian–Bashkirian). Furthermore, REE contents and various elemental ratios of these rims show a relatively homogeneous composition, which suggests that the process of zircon crystallization was by dissolution–precipitation. The compositional difference between the two analysed samples (349 and 524) observed in Eu/Eu* and Ce/Sm suggests that zircon rims from sample 349 precipitated from less evolved melts than those of sample 524, which precipitated from possibly less oxidized melts that had undergone substantial feldspar crystallization.

The late intrusion of the composite Sant Llorenç–La Jonquera plutonic complex (314–311 Ma) and the Ceret stock (312–307 Ma) was coeval with D_2. The Sant Llorenç–La Jonquera plutonic sheet was emplaced between the medium-grade Upper Proterozoic–Lower Cambrian series and the low-grade Upper Ordovician–Silurian metasediments. At the base of the La Jonquera sheet, tonalite magmas intruded between 314.2 ± 1.5 (core ages) and 311.0 ± 0.9 Ma (rim ages). The ages are significantly older than the age previously estimated (282 ± 5 Ma on Rb–Sr whole-rock, Cocherie 1984; 295 ± 7 Ma on U–Pb zircon, Maurel 2003). The variable REE contents of zircons (Fig. 9c), the heterogeneous patterns of the core analyses and the relatively homogeneous patterns of the rims together with the variable size of the Eu and Ce anomalies support the interpretation of zircon cores as antecrysts. The gabbro–diorite Ceret stock intruded into lower crustal levels of the Upper Proterozoic–Lower Cambrian series. Two magmatic pulses are revealed by CL (Fig. 4), and are also demonstrated by the trace

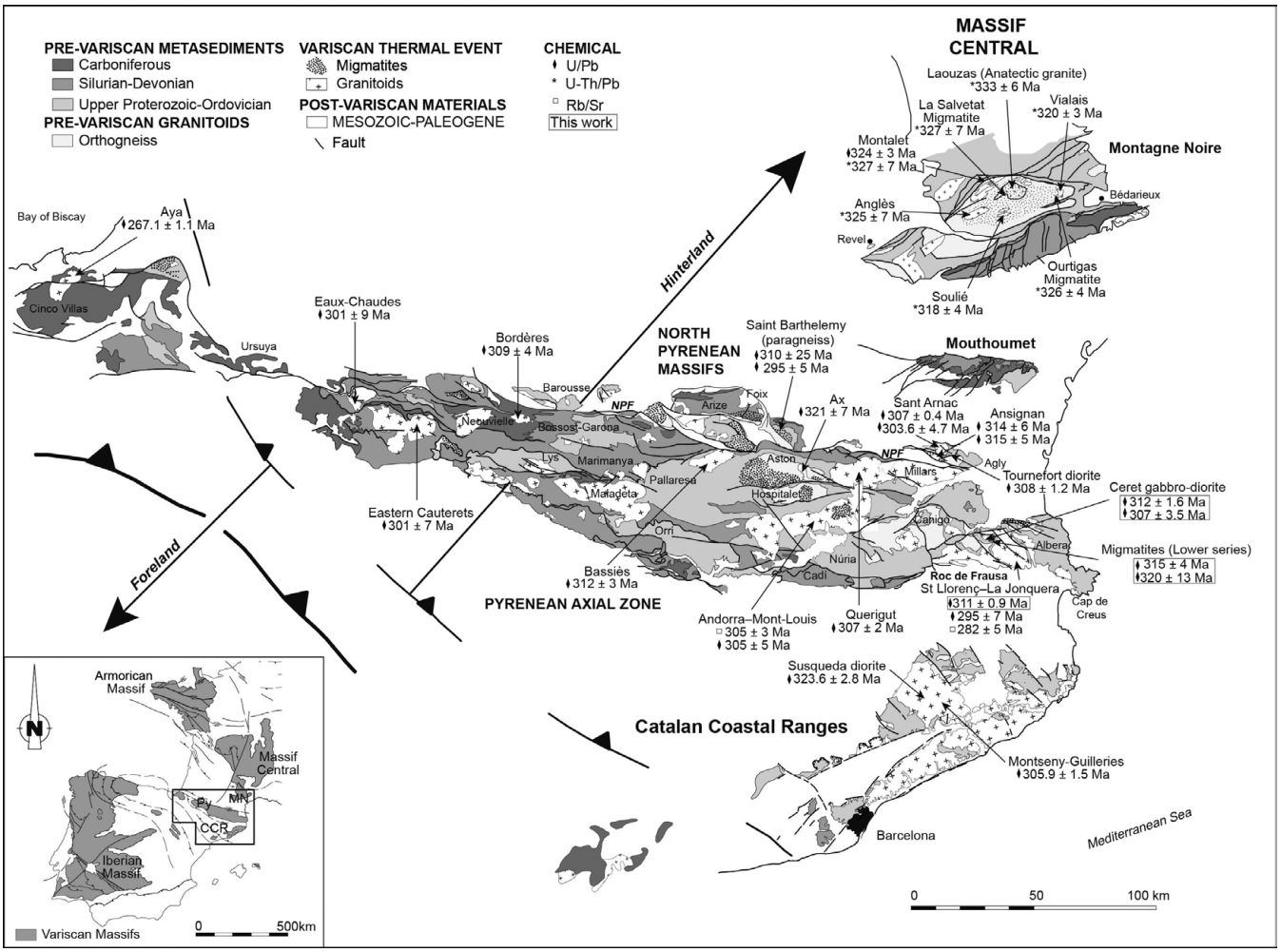

Fig. 11. Sketch of the Variscan zonation in NE Iberia and southern France, modified from Druguet (2001), with the available ages of the migmatites and intrusive rocks. NPF, North Pyrenean Fault; Py, Pyrenees; CCR, Catalan Coastal Ranges; MN, Montagne Noire.

element compositional differences between non-luminescent cores and luminescent rims of zircons (Fig. 10). The non-luminescent cores correspond to an early magmatic pulse that occurred at 312 ± 1.6 Ma. They grew from a more evolved magma where most of the plagioclase had already crystallized, in accordance with the lower values for Eu anomalies. The young ages obtained from the cores (307.6 ± 1.5 Ma) probably represent lead loss. The luminescent rims correspond to a second pulse that took place at 307.0 ± 3.5 Ma. They originated from a second and less evolved magma where plagioclase had not completely crystallized, as suggested by the lower Hf content and the shallower Eu anomaly (Fig. 10a). The absence of meso- and microscopic evidence of physical mixing (mingling) suggests that the mixture was complete; therefore, the existence of these two magmatic pulses is recorded only in zircon. In summary, zircon geochemistry suggests a complex magmatic history for the Sant Llorenç–La Jonquera suite and the gabbro–diorite Ceret stock. This history includes several pulses of magma and mixing of magmas with different geochemical characteristics. Moreover, the chemistry of zircon supports the proposal of Vilà *et al.* (2005) that these two igneous bodies are geochemically diverse and they belong to genetically distinct igneous suites produced in different levels of the lithosphere.

In the migmatites from the Ceret gabbro contact aureole, Variscan rims around inherited zircon are absent. This suggests that zirconium was retained in the pre-existing zircon grains and was barely dissolved during the migmatization event, with the result that isotopic re-equilibration was incomplete.

Comparison with the Variscan segment of the Pyrenees

The late Variscan crustal heating recorded in the eastern Pyrenees has also been observed in the more western parts of the Pyrenees, such as the deep-seated intrusive rocks of the Ax granite in the Aston Massif and the deformed deep-seated granite and charnockite in the Agly Massif (Fig. 11). They yield ages between 321 and 314 Ma (Table 1) similar to those obtained for the early partial melting episode recorded in the deepest migmatites of the Roc de Frausa Massif (320–315 Ma). However, younger U–Pb ages (310 ± 25 and 295 ± 5 Ma) have been obtained for the deepest granulitic paragneisses of the Saint Barthelemy Massif (Delaperrière *et al.* 1994).

This episode was followed by the emplacement of mafic rocks in the middle crust subordinate to large calc-alkaline plutons in the upper crust. Few geochronological data are available for the former. In the Agly Massif, the Tournefort diorite yields a U–Pb age of 308.3 ± 1.2 Ma (Olivier *et al.* 2008). This age is younger than that

Table 1. *Available ages for migmatites and intrusive rocks of the Variscan Belt in the Pyrenees, Montagne Noire and Catalan Coastal Ranges*

Locality	Age (Ma)	Reference	Method	Technique
PYRENEES				
Migmatites				
Roc de Frausa Massif				
Migmatites (Lower Series)	320±13	This study	U–Pb zircon	SHRIMP-RG
	315±4	This study	U–Pb zircon	SHRIMP-RG
Saint Barthelemy				
Paragneiss	310±25	Delaperrière *et al.* 1994	U–Pb zircon or monazite	
	295±5	Delaperrière *et al.* 1994	U–Pb zircon or monazite	
Deep crustal intrusive rocks				
Aston Massif				
Ax granite	321±7	Denèle *et al.* 2007	U–Pb zircon	
Agly Massif				
Deformed deep-seated granite	317±3	Olivier *et al.* 2004	U–Pb zircon	ID-TIMS
Ansignan charnockite	314±6	Respaut & Lancelot 1983	U–Pb zircon	
	315±5	Postaire 1984	U–Pb zircon	
Mid-crustal intrusive rocks				
Agly Massif				
Tournefort diorite	308.3±1.2	Olivier *et al.* 2008	U–Pb zircon	ID-TIMS
Roc de Frausa Massif				
Ceret gabbro	312±1.6	This study	U–Pb zircon	SHRIMP-RG
	307.6±1.5	This study	U–Pb zircon	SHRIMP-RG
	307±3.5	This study	U–Pb zircon	SHRIMP-RG
Calc-alkaline upper-crustal intrusive rocks				
La Jonquera–Sant Llorenç	282±5	Cocherie 1984	Whole-rock Rb/Sr	
	295±7	Maurel 2003	U–Pb zircon	SIMS
	314.2±1.5	This study	U–Pb zircon	SHRIMP-RG
	311.0±0.9	This study	U–Pb zircon	SHRIMP-RG
Saint Arnac	303.6±4.7	Olivier *et al.* 2008	U–Pb zircon	ID-TIMS
Querigut	307±2	Roberts *et al.* 2000	U–Pb zircon	
Andorra, Mont-Louis	305±3	Romer & Soler 1995	U–Pb titanite	
	305±5	Maurel *et al.* 2004	U–Pb zircon	SIMS
Bassiès	312±3	Paquette *et al.* 1997	U–Pb zircon	
Eastern Cauterets	301±7	Ternet *et al.* 2004	U–Pb zircon	
Eaux-Chaudes	301±9	Ternet *et al.* 2004	U–Pb zircon	
Bordères	309±4	Gleizes *et al.* 2006	U–Pb zircon	SIMS
Aya (alkaline)	267.1±1.1	Denèle *et al.* 2011	U–Pb zircon	LA-ICP-MS
MONTAGNE NOIRE				
Migmatites				
La Salvetat	327±7	Faure *et al.* 2010	U–Th–Pb monazite	EPMA
Ourtigas	326±4	Faure *et al.* 2010	U–Th–Pb monazite	EPMA
Anatectic granite				
Laouzas	333±6	Faure *et al.* 2010	U–Th–Pb monazite	EPMA
Montalet granite	324±3	Faure *et al.* 2010	U–Pb zircon	SIMS
	327±7	Faure *et al.* 2010	U–Th–Pb monazite	EPMA
Late to post-migmatitic granite				
Anglès	325±7	Faure *et al.* 2010	U–Th–Pb monazite	EPMA
Vialais	320±3	Faure *et al.* 2010	U–Th–Pb monazite	EPMA
Soulié	318±4	Faure *et al.* 2010	U–Th–Pb monazite	EPMA
CATALAN COASTAL RANGES				
Montseny–Guilleries Massif				
Susqueda diorite	323.6±2.8	Martínez *et al.* 2008	U–Pb zircon	SHRIMP-RG
Granite	305.9±1.5	Martínez *et al.* 2008	U–Pb zircon	SHRIMP-RG
Leucogranite	305.3±1.9	Martínez *et al.* 2008	U–Pb zircon	SHRIMP-RG
	301.5±1.7	Martínez *et al.* 2008	U–Pb zircon	SHRIMP-RG
	299.0±2.3	Martínez *et al.* 2008	U–Pb zircon	SHRIMP-RG

ID-TIMS, isotope dilution thermal ionization mass spectrometry; SIMS, secondary ionization mass spectrometry; LA-ICP-MS, laser ablation inductively coupled plasma mass spectrometry; EPMA, electron microprobe analysis.

of the first magmatic pulse of the Ceret gabbro–diorite (312 ± 1.6 Ma, recorded in the antecrystic cores) but comparable with the second one, dated at 307.0 ± 3.5 Ma (recorded in the rims). The emplacement of the large upper crustal calc-alkaline plutons of the Pyrenees could have lasted for about 15 myr. This episode could have been diachronous (314–301 Ma) along the Pyrenees. The ages obtained in this study for the Sant Llorenç–La Jonquera plutonic complex are in the older range if we consider those yielded by recent studies on other calc-alkaline intrusive bodies of the Pyrenees (between 312 to 301 Ma; see Fig. 11 and Table 1). Moreover, the ages obtained in this study record a multiple intrusion history that has not been reported to date.

Correlation with the Variscan segment of Montagne Noire (SE France) and the Catalan Coastal Ranges (NE Iberia)

It is tempting to correlate the observations from the Pyrenean Variscides with those of the neighbouring areas such as Montagne Noire and the Catalan Coastal Ranges. The available data for migmatites and intrusive rocks (Table 1) point to older ages and longer thermal histories to the NE (Fig. 11). The chronological relationships between the migmatitic and magmatic episodes could indicate a zonation consistent with the foreland propagation of the orogen from NE to SW. Similarly, the time–space distribution of migmatites and plutons along the Pyrenees, the Coastal Ranges and Montagne Noire is in line with the relative position of the hinterland and foreland of the southern branch of the Variscan belt, corresponding to the south-western polarity of Variscan structures in the three areas (Martínez Catalán 1990; Carreras & Debat 1996; Matte 2001).

Conclusions

New U–Pb SHRIMP zircon dating on late Variscan migmatites and igneous rocks from the eastern Pyrenees, combined with trace element chemistry of zircon, allowed us to see two episodes in the thermal evolution of the area. The first, an early migmatization in the deepest crustal levels of Roc de Frausa Massif, occurred during the Serpukhovian–Bashkirian (320–315 Ma) over a time span of *c.* 5 myr, coeval with the main deformation event (D_1). This thermal episode is also responsible for the intrusion of deep-seated granitoids in other Pyrenean massifs (Agly and Aston). The second episode, late intrusion during the Late Bashkirian–Moscovian (314–307 Ma) synchronous with a late deformation event (D_2), corresponds to the emplacement of the calc-alkaline La Jonquera–Sant Llorenç plutonic complex and the Ceret gabbro–diorite stock in upper and middle crustal levels, respectively. CL, transmitted light microscope and trace element chemistry of zircon show that two magmatic pulses can be recorded in the Ceret gabbro–diorite separated by a time span of *c.* 5 myr. Migmatites were formed around the Ceret gabbro contact aureole but the absence of Variscan rims around inherited zircon prevented us from dating the episodes. Space–time correlation of the Pyrenees with neighbouring areas (Catalan Coastal Ranges and Montagne Noire) allows us to construct a NW–SE-trending zonation model.

This work has funded by the research projects CGL2007-66857-C02-02 and CGL2010-21298 of the Spanish Ministerio de Ciencia e Innovación (MICINN). The work forms part of a PhD thesis by C.A. The Spanish MICINN provided an FPI grant (BES-2008-001841), which included a 3 month stay (SEST1000I000682XV0) at Stanford University during 2010. We are grateful to J. Wooden, J. Vazquez and B. Ito of the SUMAC staff at Stanford University for the close supervision of zircon-mount preparations and imaging, zircon analyses and instrument tuning. We are indebted to J. A. Muñoz and J. M. Casas for invaluable comments on the paper. We are also grateful to J. von Raumer for his detailed and constructive criticism and for his help with the final version of the paper, and to an anonymous referee. G. von Knorring reviewed the English style of the paper.

References

Anders, E. & Grevesse, N. 1989. Abundances of the elements: Meteoritic and solar. *Geochimica et Cosmochimica Acta*, **53**, 197–204.

Autran, A. & Guitard, G. 1969. Mise en évidence de nappes hercyniennes de style penninique dans la série métamorphique du massif du Roc de France (Pyrénées orientales): Liaison avec la nappe du Canigou. *Comptes Rendus de l'Académie des Sciences*, **269**, 2479–2499.

Carreras, J. & Debat, P. (coords) 1996. La Tectonique Hercynienne. *In*: Barnolas, A. & Chiron, J.C. (eds) *Synthèse géologique et géophysique des Pyrénées. Vol. 1: Introduction. Géophysique. Cycle Hercynien*. Édition BRGM-ITGE, Orléans and Madrid, 585–677.

Castiñeiras, P., Navidad, M., Liesa, M., Carreras, J. & Casas, J.M. 2008. U–Pb zircon ages (SHRIMP) for Cadomian and Early Ordovician magmatism in the eastern Pyrenees: New insights into the pre-Variscan evolution of the northern Gondwana margin. *Tectonophysics*, **461**, 228–239.

Charlier, B.L.A., Wilson, C.J.N., Lowenstern, J.B., Blake, S., Vancalsteren, P.W.C. & Davidson, J.P. 2005. Magma generation at a large, hyperactive silicic volcano (Taupo, New Zealand) revealed by U–Th and U–Pb systematics in zircons. *Journal of Petrology*, **46**, 3–32.

Cirés, J., Morales, V., Liesa, M., Carreras, J., Carreras, J., Escuer, J. & Pujadas, J. 1994. *Memoria explicativa del mapa geológico de España, hoja de La Jonquera (220), scale 1:50000*. Instituto Tecnológico Geominero de España, Madrid.

Cocherie, A. 1984. *Interaction manteau–croûte: Son rôle dans la génèse d'associations plutoniques calco-alcalines, contraintes géochimiques (élements en traces et isotopes du strontium et de l'oxygène)*. PhD thesis, Universitè de Rennes.

Debon, F., Enrique, P. & Autran, A. 1995. Magmatisme Hercynian. *In*: Barnolas, A. & Chiron, J.C. (eds) *Synthèse géologique et géophysique des Pyrénées. Vol. 1: Introduction. Géophysique. Cycle Hercynien*. Édition BRGM-ITGE, Orléans and Madrid, 303–359.

Delaperrière, E., De Saint-Blanquat, M., Brunel, M. & Lancelot, J. 1994. Géochronologie U–Pb sur zircons et monazites dans le massif du Saint Barthelemy (Pyrénées, France): Discussion des âges des événements variues et pré-varisques. *Bulletin de la Société Géologique de France*, **165**, 101–112.

Denèle, Y., Olivier, P., Gleizes, G. & Barbey, P. 2007. The Hospitalet gneiss dome (Pyrénées) revisited: lateral flow during Variscan transpression in the middle crust. *Terra Nova*, **19**, 445–453.

Denèle, Y., Paquette, J.L., Olivier, PH. & Barbey, P. 2011. Permian granites in the Pyrenees: the Aya pluton (Basque Country). *Terra Nova*, **24**, 105–113.

Druguet, E. 2001. Development of high thermal gradients by coeval transpression and magmatism during the Variscan orogen: Insights from the Cap de Creus (eastern Pyrenees). *Tectonophysics*, **332**, 275–293.

Faure, M., Cocherie, A., Bémézème, E., Charles, N. & Rossi, P. 2010. Middle Carboniferous crustal melting in the Variscan Belt: New insights from U–Th–$Pb_{tot.}$ monazite and U–Pb zircon ages of the Montagne Noire Axial Zone (southern French Massif Central). *Gondwana Research*, **18**, 653–673.

Gleizes, G., Crevon, G., Asrat, A. & Barbey, P. 2006. Structure, age and mode of emplacement of the Hercynian Bordères–Louron pluton (central Pyrenees, Frances). *International Journal of Earth Sciences*, **95**, 1039–1052.

Guitard, G., Vielzeuf, D. & Martínez, F. 1995. Métamorphisme Hercynian. *In*: Barnolas, A. & Chiron, J.C. (eds) *Synthèse géologique et géophysique des Pyrénées. Vol. 1: Introduction. Géophysique. Cycle Hercynien*. Édition BRGM-ITGE, Orléans and Madrid, 303–359.

Holland, T.J.B. & Powell, R. 1998. An internally-consistent thermodynamic data set for phases of petrologic interest. *Journal of Metamorphic Geology*, **16**, 309–343.

Korotev, R.L. 1996. A self-consistent compilation of elemental concentration data for 93 geochemical reference samples. *Geostandards Newsletter*, **20**, 217–245.

Liesa, M. & Carreras, J. 1989. On the structure and metamorphism of the Roc de Frausa Massif (eastern Pyrenees). *Geodinamica Acta*, **3**, 149–161.

Martínez, F.J., Reche, J. & Iriondo, A. 2008. U–Pb SHRIMP-RG zircon ages of Variscan igneous rocks from the Guilleries Massif (NE Iberia pre-Mesozoic basament). Geological implications. *Comptes Rendus Géosciences*, **340**, 223–232.

Martínez Catalán, J.R. 1990. A non-cylindrical model for the northwest Iberian allochthonous terranes and their equivalents in the Hercynian belt of western Europe. *Tectonophysics*, **179**, 253–272.

Matte, PH. 2001. The Variscan collage and orogeny (480–290 Ma) and the tectonic definition of the Armorica microplate: a review. *Terra Nova*, **13**, 122–128.

Maurel, O. 2003. *L'exhumation de la Zone Axiale des Pyrénées orientales: une approche thermo-chronologique multi-méthodes du rôle des failles*. PhD thesis, Université de Montpellier.

Maurel, O., Respaut, J.P., Monié, P., Arnaud, N. & Brunel, M. 2004. U–Pb emplacement and $^{40}Ar/^{39}Ar$ cooling ages of the eastern Mont-Louis granite massif (eastern Pyrenees, France). *Comptes Rendus Geosciences*, **336**, 1091–1098.

Olivier, PH., Gleizes, G. & Paquette, J.L. 2004. Gneiss domes and granite emplacement in an obliquely convergent regime: New interpretation of the Variscan Agly Massif (eastern Pyrenees, France). *In*: Whitney, D.L., Teyssier, C. & Siddoway, C.S. (eds) *Gneiss Domes in Orogeny*. Geological Society of America, Special Paper, **380**, 229–242.

Olivier, Ph., Gleizes, G., Paquette, J.L. & Muñoz-Sáez, C. 2008. Structure and U–Pb dating of the Saint-Arnac pluton and the Ansignan charnockite (Agly Massif): A cross-section from the upper to the middle crust of the Variscan eastern Pyrenees. *Journal of the Geological Society, London*, **165**, 141–152.

Paquette, J.L., Gleizes, G., Leblanc, D. & Bouchez, J.L. 1997. Le granite de Bassiès (Pyrénées): Un pluton syntectonique d'âge Westphalien. Géochronologie U–Pb sur zircons. *Comptes Rendus de l'Académie des Sciences*, **324**, 387–392.

Postaire, B. 1984. Systématique Pb commun et U–Pb sur zircons: Applications aux roches de haut grade métamorphique impliquées dans la chaîne hercynienne (Europe de l'ouest) et aux granulites de Laponie (Finlande). *Mémoires de la Société Géologique et Minéralogique de Bretagne*, **15**, 29–72.

Respaut, J.P. & Lancelot, J.R. 1983. Datation de la mise en place synmétamorphe de la charnockite d'Ansignan (massif de l'Agly) par la méthode U/Pb sur zircons et monazites. *Neues Jahrbuch für Mineralogie*, **147**, 21–34.

Roberts, M.P., Pin, C., Clemens, J.D. & Paquette, J.L. 2000. Petrogenesis of mafic to felsic plutonic rock associations: The calc-alkaline Quérigut complex, French Pyrenees. *Journal of Petrology*, **41**, 809–844.

Romer, R.L. & Soler, A. 1995. U–Pb age and lead isotopic characterization of Au-bearing skarn related to the Andorra granite (central Pyrenees, Spain). *Mineralium Deposita*, **30**, 374–383.

Sambridge, M.S. & Compston, W. 1994. Mixture modeling of multi-component data sets with application to ion-probe zircon ages. *Earth and Planetary Science Letters*, **128**, 373–390.

Ternet, Y., Majesté-Menjoulas, C., Canérot, J., Baudin, T., Cocherie, A., Guerrot, C. & Rossi, P. 2004. *Notice Explicative, Carte géologique de la France (1/50000), feuille Laruns-Somport (1069)*. BRGM, Orléans.

Vilà, M., Pin, C., Enrique, P. & Liesa, M. 2005. Telescoping of three distinct magmatic suites in an orogenic setting: Generation of Hercynian igneous rocks of the Albera Massif (eastern Pyrenees). *Lithos*, **83**, 97–127.

Wendt, I. & Carl, C. 1991. The statistical distribution of the mean squared weighted deviation. *Chemical Geology*, **86**, 275–285.

Zwart, H.J. 1962. On the determination of polymetamorphic mineral association and its application to the Bossost area (central Pyrenees). *Geologische Rundschau*, **52**, 38–65.